Catalysis Today 168 (2011) 133–139

Contents lists available at ScienceDirect

Catalysis Today

journal homepage: www.elsevier.com/locate/cattod

Design of hierarchically structured catalysts by mordenites recrystallization: Application in naphthalene alkylation

I.I. Ivanova[a,*], A.S. Kuznetsov[a], E.E. Knyazeva[a], F. Fajula[b], F. Thibault-Starzyk[c], C. Fernandez[c], J.-P. Gilson[c]

[a] Department of Chemistry, Moscow State University, Lenin Hills, 119991 Moscow, Russia
[b] Institut Charles Gerhardt Montpellier, UMR 5253 CNRS, UM2, ENSCM, 8 Rue de l'Ecole Normale, 34296 Montpellier Cedex, France
[c] Laboratoire Catalyse et Spectrochimie, ENSICAEN, Université de Caen, CNRS, 6 bd du Maréchal Juin, 14050 Caen, France

ARTICLE INFO

Article history:
Received 7 October 2010
Received in revised form
27 November 2010
Accepted 29 November 2010
Available online 7 January 2011

Keywords:
Mesoporous mordenite
Micro–mesoporous composite materials
Naphthalene alkylation with cyclohexene
Alkylnaphthalenes

ABSTRACT

Micro/mesoporous composite materials with different levels of micro- and mesoporosity were prepared by recrystallization of mordenite in the presence of cethyltrimethylammonium bromide. The materials were characterized by XRD, TEM, IR spectroscopy, nitrogen adsorption–desorption and NH_3-TPD. The results highlight that recrystallization in mild condition results in the creation of mesopores in the zeolite crystals and their coating with thin films of mesoporous material. The increase of the degree of recrystallization leads first to the formation of composite materials MOR/MCM-41 and then to a complete transformation of mordenite in MCM-41, followed by a gradual decrease of the amount and strength of acid sites. Recrystallized materials display remarkably high activity, stability and selectivity in alkylation of naphthalene with cyclohexene. The effect is due to the improved accessibility of active sites and easier transport of bulky molecules provided by mesopores. The best catalytic performance is achieved on composite materials with intermediate degree of recrystallization. The yield of alkylnaphthalenes over these materials reaches 80%, while the yield of monoalkylnaphthalenes is up to 58%.

1. Introduction

The rational design of zeolite catalysts requires a controlled tailoring of their pore architecture as well as the mastering of the nature, strength and localization of their active sites in the porous system. While the methods for tuning the nature and strength of the active sites are well established, pore architecture and localization of active sites is usually difficult to control.

For zeolite catalysts, it has been repeatedly demonstrated that mass transfer limitations play an important role in many of their industrial applications. Creation of mesoporosity can minimize or even cancel these limitations [1]. In the last few years, much effort was dedicated to the development of the novel class of molecular sieves with bimodal micro–mesoporous structure [2–6]. These materials were expected to combine the advantages of both mesoporous molecular sieves and zeolites, namely, improved transport of bulky molecules with high zeolitic acidity and hydrothermal stability.

Several approaches were used for the design of such materials. A first approach involves conventional dealumination procedures, such as calcination, steaming, acid leaching or combined treatments [7–9]. Another approach, widely applied recently, is based on the opposite strategy of desilication by alkaline treatments [10,11]. Both procedures lead to creation of mesopores in zeolitic crystals.

In another methodology, matrix assisted synthesis, first reported by Jacobsen et al. [12], a mesoporous carbon matrix is impregnated with a reaction mixture for zeolite synthesis and the crystals are grown around the carbon particles. The subsequent calcination of the encapsulated carbon matrix leads to isolated large zeolite crystals with a uniform mesopore system.

An alternative approach involves the synthesis of mesoporous materials from tiny zeolitic species in two steps: (i) the preparation of tiny zeolite seeds during a short hydrothermal step, (ii) their assembly into mesoporous material during a second hydrothermal reaction in the presence of surfactant [13,14].

The opposite strategy proposed by van Bekkum and co-workers [15] and Kaliagine [16,17] is based on the transformation of preassembled walls of mesoporous materials such as MCM-41 and SBA-15 into zeolitic structures by post-assembly treatment with a zeolite structure directing template. The walls of such materials are indeed partially recrystallized into zeolite, as evidenced by TEM images. A related approach, also adopted by Kaliagine and coworkers [18], includes the coating of mesoporous materials with nanozeolite seeds using very diluted clear zeolite gels.

* Corresponding author.
E-mail address: iiivanova@phys.chem.msu.ru (I.I. Ivanova).

0920-5861/$ – see front matter © 2010 Published by Elsevier B.V.
doi:10.1016/j.cattod.2010.11.091

Table 1
Characteristics of parent and recrystallized mordenites.

Samples	C_{NaOH} (M)	Na/Al	Si/Al	V (cm^3/g)	V_{mic} (cm^3/g)	V_{mic}/V[a]
MOR	–	>0.01	48	0.246	0.180	0.73
ReMOR-0.5	0.4	0.12	66	0.321	0.157	0.49
ReMOR-0.4	0.48	0.11	68	0.353	0.144	0.41
ReMOR-0.3	0.55	0.53	69	0.398	0.128	0.32
ReMOR-0.2	0.65	0.05	67	0.472	0.098	0.21
ReMOR-0.1	0.8	0.05	43	0.551	0.071	0.13
ReMOR-0.0	1.2	0.07	74	0.656	0.012	0.02

[a] V_{mic}/V-contribution of microporosity.

Another interesting procedure involves a partial dissolution of zeolites in highly alkaline media, followed by recrystallization into a mesostructure [19–24]. The degree of recrystallization, the ratio of micro- and mesopores as well as structural and textural characteristics of such materials is controlled by the alkalinity of the reaction mixture. Catalysts derived from such composite materials show superior performances (activity, stability and selectivity) with respect to both pure microporous and pure mesoporous counterparts in a number of catalytic reactions such as alkylation and disproportionation of aromatic compounds, cracking of alkylaromatics, aromatization and hydroisomerization of alkanes [23].

This paper is devoted to the design of hierarchically structured catalysts for the selective alkylation of naphthalene (N) with cyclohexene (CH) using the recrystallization strategy.

2. Experimental

The parent dealuminated mordenite (MOR) used for recrystallization was supplied by Zeolyst (CBV90). The recrystallization procedure included two steps [22]: (i) first partial dissolution of the zeolite in NaOH aqueous solution at room temperature, (ii) then hydrothermal treatment in the presence of cethyltrimethylammonium bromide at 100 °C. A series of samples was prepared by varying the NaOH concentration of step (i) as shown in Table 1.

The organic template was removed by calcination in a flow of dry air at 550 °C for 24 h. The samples were then subjected to a twofold ion exchange in aqueous solution of ammonium nitrate (0.1 M, 50 ml) and calcination in a dry air flow at 550 °C for 6 h. The characteristics of the samples prepared are presented in Table 1. The materials obtained are denoted as ReMOR-0.5 – 0, where "ReMOR" stands for recrystallized mordenite and the indexes 0.5 – 0 correspond to the contribution of microporosity in the sample, i.e. V_{micro}/V ratio shown in Table 1.

The chemical composition of the samples was determined by atomic emission spectroscopy (AES). X-ray diffraction (XRD) patterns were recorded using a Bruker D8 Advance diffractometer, applying CuK_α radiation and operating at 40 kV and 20 mA. Crystallite sizes were calculated following the Williamson–Hall method [25]. The relative crystallinity of the samples was estimated from the integrated intensity of the 10 most intense diffraction peaks in the region 5–30 $2\theta^\circ$ using the parent dealuminated mordenite (MOR) as reference for 100% crystallinity. Prior to be mounted on the X-ray probe the samples were allowed to rehydrate under ambient atmosphere, gently ground in a mortar to avoid particle aggregation and precisely weighted.

Sorption–desorption isotherms of nitrogen were measured at −196 °C using an automated porosimeter (Micromeritics ASAP 2000). Micropore volumes were determined using the *t*-plot method. The total volume sorbed, (micropores, mesopores and on the external surface) were calculated from the amount of nitrogen adsorbed at relative pressure p/p_0 of 0.95, before the onset of interparticle condensation.

Transmission electron microscopy images (TEM) were obtained using a JEOL 1200 EX II electron microscope, operating at 100 kV. Samples were placed on a microgrid carbon polymer supported on a copper grid by depositing of few droplets of a suspension of ground sample in ethanol on the grid, followed by drying at ambient conditions.

The acidic properties were studied by temperature programmed desorption of ammonia (NH_3-TPD) and IR-spectroscopy of adsorbed probe molecules. NH_3-TPD was performed in a home-made set up equipped with TC detector. Prior to NH_3 adsorption, the samples were calcined *in situ* in a flow of dry air at 550 °C for 1 h and, subsequently, in a flow of dry nitrogen for 1 h and cooled down to ambient temperature. The NH_3 adsorption was carried out during 30 min, at ambient temperature in a flow of NH_3 diluted with N_2 (1/1). Subsequently, the physically adsorbed NH_3 was removed in a flow of dry He at 100 °C for 1 h. Typical TPD experiments were carried out in the temperature range of 20–780 °C in a flow of dry He (30 ml/min). The rate of heating was 8 °C/min.

IR spectra were recorded with a Vector 22 (Bruker) equipped by DTGS detector at 4 cm^{-1} optical resolution. Prior to the measurements, the catalysts were pressed in self-supporting discs (diameter: 1.6 cm, 10 mg/cm^2) and activated at 450 °C (heating rate 1 °C/min) for 6 h up to 10^{-6} Torr in the IR cell. Pyridine (Py) and collidine (Coll) adsorption was performed at 200 °C. After adsorption, the excess of probe molecules was evacuated. The adsorption–evacuation was repeated several times until no changes in the spectra were observed. Molar absorbance coefficients for probe molecules were used as described in Ref. [26]. More general description of the use of probe molecules to characterise active sites is described in Ref. [27].

Catalytic experiments were performed in a continuous flow fixed bed reactor system. The reaction conditions, optimized in a previous study [28], were as follows: $T = 160$ °C, $P = 10$ atm, $WHSV_N = 0.5\ h^{-1}$ and molar ratio CH:N:N_2 = 1:1:10. The reaction was carried out in the presence of decaline, acting as a solvent. The analysis of the gaseous products was performed on a KCl/Al_2O_3 capillary column (80 m × 0.22 mm), while liquid products were analyzed using 50 m capillary column SE-30.

3. Results and discussion

3.1. Structure and texture of recrystallized zeolites

The tuning of structural and textural characteristics of the materials during recrystallization was achieved by varying the degree of alkalinity, previously shown to be the most important parameter [19,21,22]. By variation of NaOH concentration in the range of 0.4–1.6 M, a series of materials with different levels of mesoporosity was obtained as shown in Table 1 (samples ReMOR-0.5–0).

The N_2 adsorption–desorption isotherms of the resulting materials (Fig. 1) show that recrystallized mordenites exhibit sharp steps at $p/p_0 \sim 0.42$, corresponding to the existence of uniform mesoporosity. Mesopore formation results in a significant increase of the pore volumes upon recrystallization (Table 1). According to the BJH analysis, the average size of the mesopores is about 30 Å.

The X-ray diffraction patterns do not show the presence of any new signals in the XRD-spectra after recrystallization, at least in 5–40 $2\theta^\circ$ region (Fig. 2). However, the intensity of the peaks decreases with the recrystallization degree, indicating that a part of the zeolite phase is irreversibly destroyed and/or transformed after dissolution in the stronger alkaline conditions. For example, sample ReMOR-0.0 contains only trace amounts of mordenite according to XRD-data.

More detailed information is obtained by the analysis of line broadening according to the Williamson-Hall method and calcula-

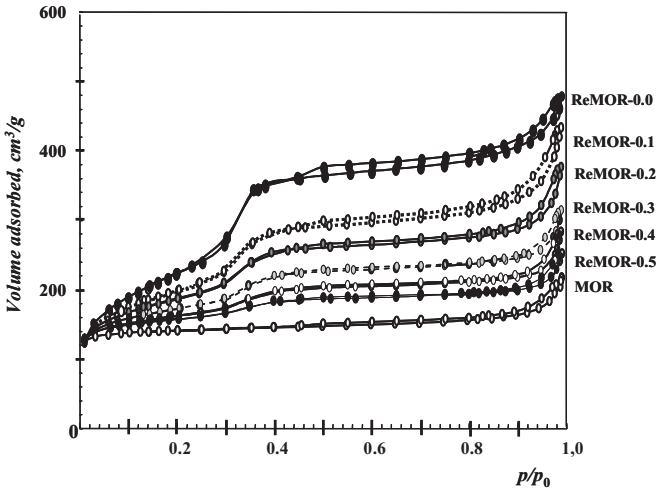

Fig. 1. Nitrogen adsorption–desorption isotherms obtained at −196 °C over parent mordenite and recrystallized materials.

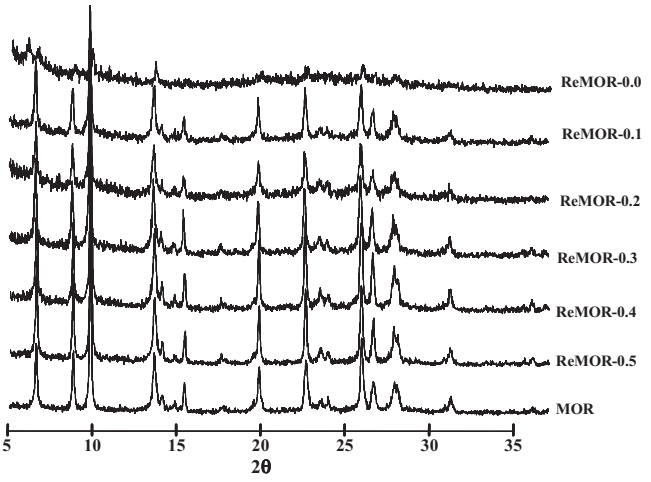

Fig. 2. Wide angle range XRD-patterns of parent mordenite and recrystallized materials.

tion of crystallinity degree of the modified samples relative to that of the parent MOR. The small width of XRD-lines for H/ReMOR-0.5–0.3 samples points to rather large (higher than ~100 nm) crystallite sizes (Fig. 3). For the H/ReMOR-0.2 and H/ReMOR-0.1

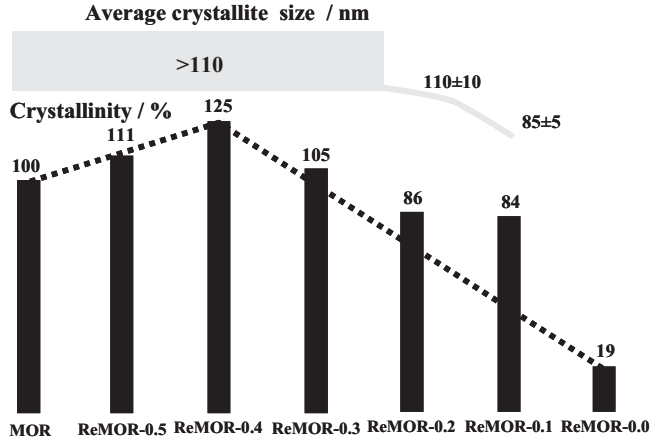

Fig. 3. Average crystallite size and relative crystallinity of parent mordenite and recrystallized materials.

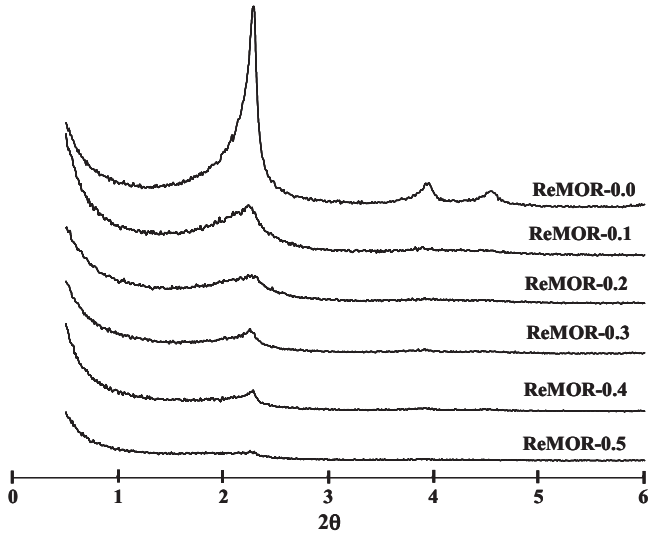

Fig. 4. Small angle XRD-patterns of parent mordenite and recrystallized materials.

samples, the crystallite size is decreasing slightly to ~80 nm with the severity of dissolution.

The relative crystallinity increases slightly for the samples obtained after recrystallization under moderate alkalinity (Fig. 3). This unusual effect is likely to be due to the dissolution of some amorphous phase contained in the parent dealuminated mordenite and/or to the recovery of some zeolitic mordenite phase due to the healing of defects in the zeolite framework under alkaline conditions. Further increase of the alkalinity leads to a loss of crystallinity, indicating a higher degree of transformation of the mordenite phase.

The investigation of the structure of the mesoporous phase was carried out by small angle X-ray diffraction. A series of characteristic peaks on the XRD patterns indicates the presence of hexagonal MCM-41 phase with a cell parameter of 39.4 Å (Fig. 4). Their intensity is the higher at higher recrystallization degrees, indicating a larger content of MCM-41 phase in the composite materials.

Further insight on the relative localization of the zeolitic and the mesoporous phases is provided by transmission electron microscopy (Fig. 5). The results reveal that three different types of materials are formed depending on the degree of recrystallization:

- under mild alkaline conditions (ReMOR-0.5, ReMOR-0.4), recrystallization results in the creation of mesopores in mordenite crystals and the coating of zeolite crystals with a thin film of worm like mesoporous material (Fig. 5a);
- the increase of the degree of recrystallization (ReMOR-0.3, ReMOR-0.2) leads to the formation of composite MOR/MCM-41 materials consisting of two co-crystallized phases (Fig. 5b);
- deep recrystallization (ReMOR-0.1, ReMOR-0) results in the complete transformation of mordenite into MCM-41 containing only few small zeolite fragments (Fig. 5c).

3.2. Acidic properties

The acidity of the recrystallized materials has been studied by NH_3-TPD and IR spectroscopy of adsorbed pyridine and collidine. The former method provides information on the number and strength of the acid sites, while the latter gives information on the nature of acid sites and their accessibility. Collidine has been used previously to characterise accessibility in hierarchical zeolites, because it can partly penetrate in the pores of the zeolites. It is very sensitive to the creation of mesopores, as shown in Ref. [26].

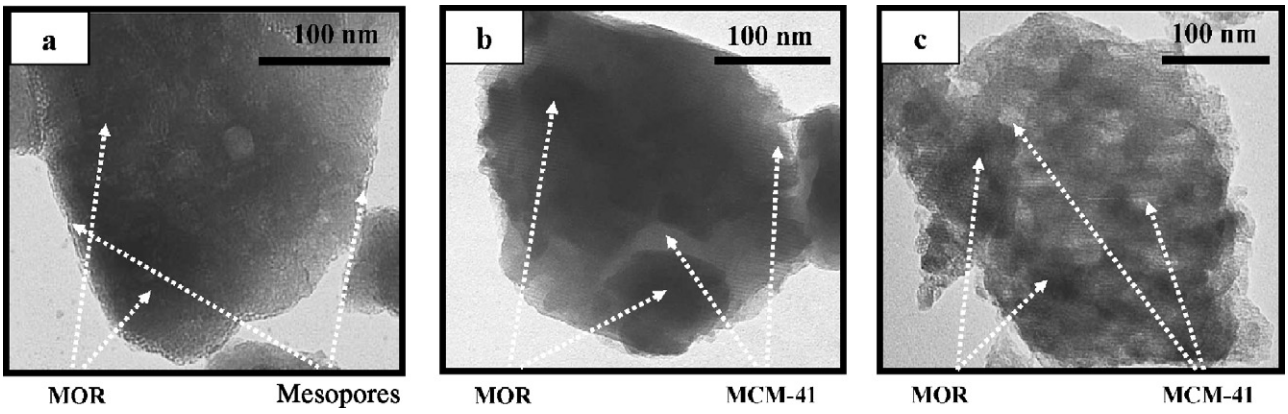

Fig. 5. TEM images of ReMOR-0.5 (a), ReMOR-0.3 (b) and ReMOR-0.1 (c).

The TPD spectra for the samples ReMOR-0.5 to ReMOR-0.1 consist of two peaks with maxima at ca. 150 and 450 °C, as in the case of parent mordenite (Fig. 6), however their intensity is modified. The intensity of the low-temperature peak decreases significantly even for the samples with low recrystallization degree. This is probably due to a faster desorption of the physisorbed ammonia due to the formation of mesopores.

The analysis of the high temperature peak suggests that ReMOR-0.5 and ReMOR-0.4 materials exhibit a strong acidity, the amount of strong acid sites on these samples being even higher than that of the parent mordenite. This result is consistent with the XRD data showing a higher degree of crystallinity for the mildly recrystallized materials and would be in line with the healing of some defects present in the parent dealuminated mordenite. Samples ReMOR-0.3 to ReMOR-0.1 also show strong acid sites, but their amount is lower than in the parent sample and decrease gradually with the degree of recrystallization. The TPD profile for a fully recrystallized mordenite (H/ReMOR-0.) is quite different: the contributions of weak and strong sites decrease significantly while the amount of sites with medium acid strength (with a maximum desorption temperature of 350 °C) increases (Fig. 6). Such a NH_3-TPD profile usually corresponds to that of Al-MCM-41 type materials.

Fig. 7 illustrates the IR-spectra of the OH-stretching region for the starting and the recrystallized mordenites. The nature of the OH-groups in recrystallized samples is similar to that of the parent mordenite. Silanol groups (3744, 3731 cm^{-1}), extra framework AlOH-groups (between 3700 and 3650 cm^{-1}), isolated (3609 cm^{-1}) Brønsted acid sites and silanol nests [29] – or more probably OH-groups interacting with extra framework aluminum species (3520 cm^{-1}) are observed for all the samples studied.

The starting mordenite contains a small amount of silanol groups. The amount of silanols increases upon recrystallization, pointing to the breaking of Al–OH–Si and Si–O–Si bonds in alkaline media.

The intensity of the Brønsted acid sites decreases especially for the samples at high recrystallization degrees. This is in good agreement with adsorption measurements, which show the decrease of the microporous volume upon recrystallization. It is interesting to note, that the intensity of the band at 3609 cm^{-1} is not zero for fully recrystallized sample – H/ReMOR-0. The preservation of Brønsted acidity in this material can be due to the presence of small domains of the mordenite type, inside the mesostructure. This can have a positive effect, not only on acidity but also on the thermal and hydrothermal stability of the mesoporous material.

A quantitative analysis of the Brønsted acid sites accessibility to different probe molecules (pyridine and the bulkier collidine) as a function of recrystallization degree is presented in Fig. 8. The amount of Brønsted acid sites accessible to pyridine does not change significantly upon recrystallization at mild conditions (H/ReMOR-0.5–0.3) but decreases significantly for the samples with high recrystallization degrees (H/ReMOR-0.2–0.0). The collidine adsorption results differ from those obtained for pyridine. The accessibility of Brønsted acid sites to collidine on partially recrystallized materials (H/ReMOR-0.5–0.3) is always higher than on the parent mordenite.

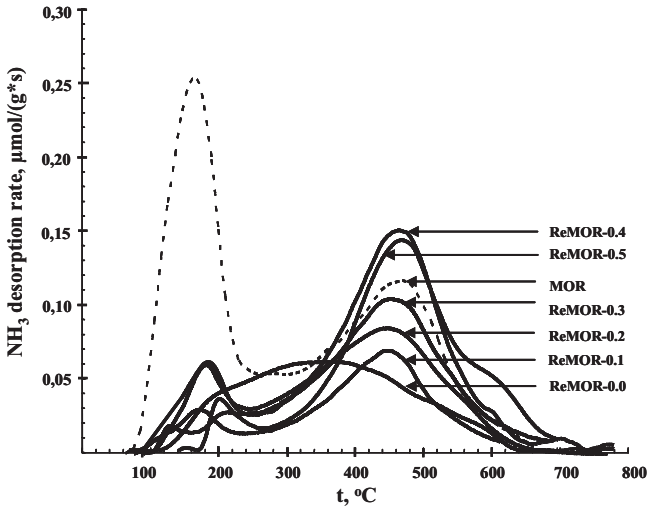

Fig. 6. NH_3 TPD spectra of parent mordenite and recrystallized materials.

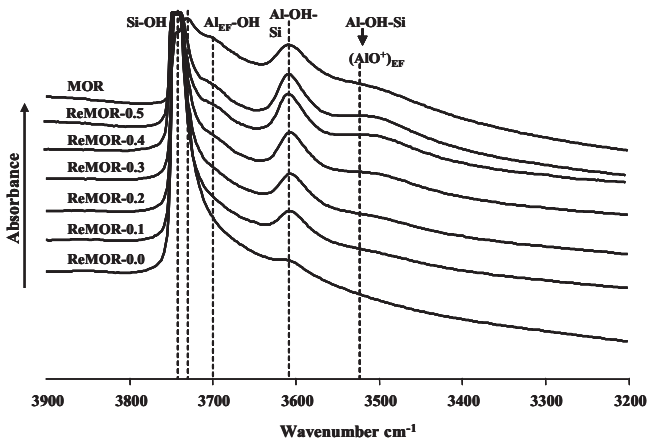

Fig. 7. OH-stretching regions of IR-spectra of parent mordenite and recrystallized materials.

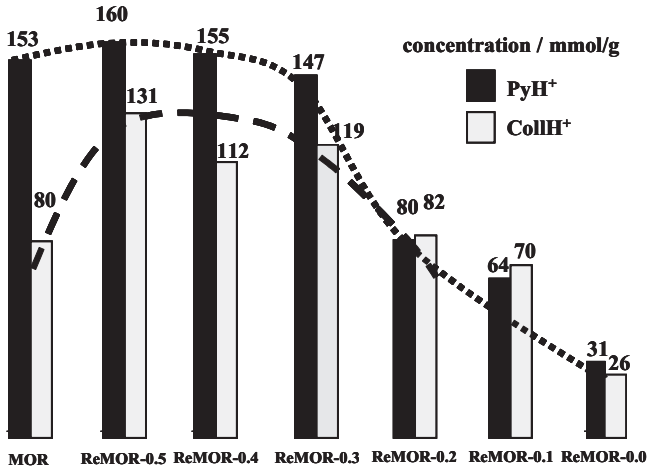

Fig. 8. Concentration of Brønsted acid sites accessible for pyridine and collidine over parent mordenite and recrystallized materials.

The increase in accessibility is well quantified by the ACI (accessibility index) [26], which increases linearly from 0.5 (50% of accessible sites) for the parent to 1 for the highest degree of recrystallization (Fig. 9). The improved acid site accessibility can be attributed to the generation of mesopores in mordenite crystals, although the loss of the zeolitic crystalline phase leads to a decrease of the total amount of acid sites. The density of Lewis acid sites, as measured with pyridines and with CO, also increases upon recrystallization; this may well have an effect on the catalytic performances as it was reported recently [30].

NH3-TPD and FTIR of adsorbed pyridine and collidine all point to the following changes in acidic properties upon recrystallization:

– $V_{mic}/V = 0.4–0.5$: the acidity is mostly due to Brønsted acid sites, their amount increases slightly, their acidic strength does not change, while their accessibility to bulky molecules such as collidine increases with respect to the starting mordenite.
– $V_{mic}/V = 0.3–0.2$: the contribution of Lewis acid sites (measured by pyridine), and silanol groups increases, the total amount of acid sites slightly decreases, the acid sites does not change while their accessibility is further improved.

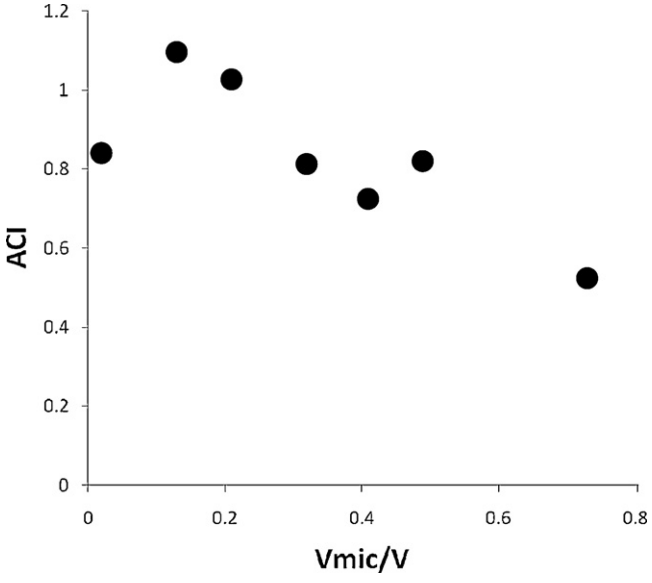

Fig. 9. Accessibility index (ACI) over parent mordenite and recrystallized materials.

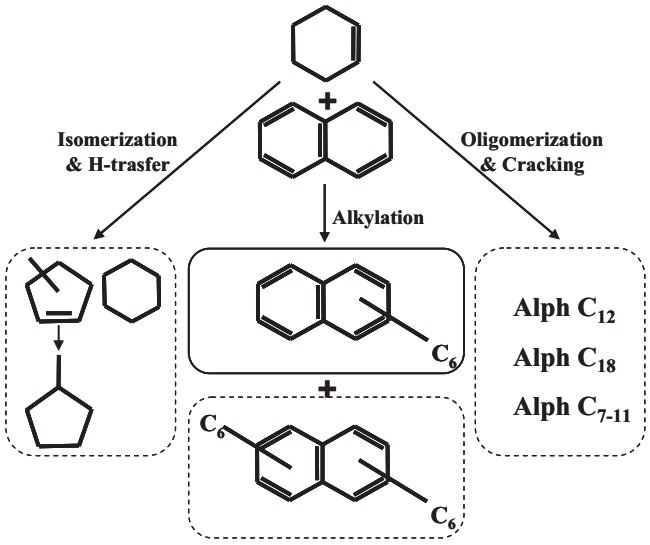

Fig. 10. Main reaction pathways observed during cyclohexene and naphthalene conversion over mordenites.

– $V_{mic}/V < 0.1$: the total number of acid sites decreases while all sites become accessible (strong Brønsted sites disappear, acidity is mostly due to Lewis sites as shown by pyridine and CO adsorption).

3.3. Catalytic properties

The products of the conversion of cyclohexene and naphthalene over the parent and recrystallized mordenites indicate that besides the formation of the target cyclohexylnaphthalene (CHN) molecule, secondary alkylation takes place leading to dicyclohexylnaphthalene (DCHN) and two parallel reaction pathways of cyclohexene conversion occur (Fig. 10):

- isomerization and hydrogenation leading to methylcyclopentenes, methylcyclopentane and cyclohexane;
- oligomerization leading to C_{12} and C_{18} aliphatic compounds (Alph C_{12} and Alph C_{18}) and cracking of the oligomers resulting in Alph C_{7-11} fraction.

The catalytic data observed over the parent and recrystallized mordenites are compared in Table 2 and Figs. 10 and 11. All micro–mesoporous catalysts display improved performances (activity and selectivity) with respect to the parent mordenite, although the catalytic properties are strongly dependent on the recrystallization degree.

Table 2
Alkylation of naphthalene with cyclohexene over parent and recrystallized mordenites ($T = 160\,^{\circ}C$, $P = 10$ atm, $WHSV_N = 0.5\,h^{-1}$, molar ration of $CH:N:N_2 = 1:1:10$, TOS = 3 h).

Catalyst	MOR	Re-MOR					
		0.5	0.4	0.3	0.2	0.1	0
Cyclohexene conversion, %	55	73	89	98	100	100	100
Naphthalene conversion, %	10	19	24	31	37	39	48
Product distribution, mol.%							
Methylcyclopentene	20	5	4	1	0	4	3
Methylcyclopentane	1	1	2	2	2	2	3
Cyclohexane	3	5	5	5	5	0	0
Alph C_7–C_{11}	2	3	2	3	1	1	1
Alph C_{12}	39	35	26	13	6	6	3
Alph C_{18}	2	3	6	6	6	7	4
Cyclohexylnaphthalene	32	43	47	55	58	55	48
Dicyclohexylnaphthalene	1	5	8	15	22	24	37

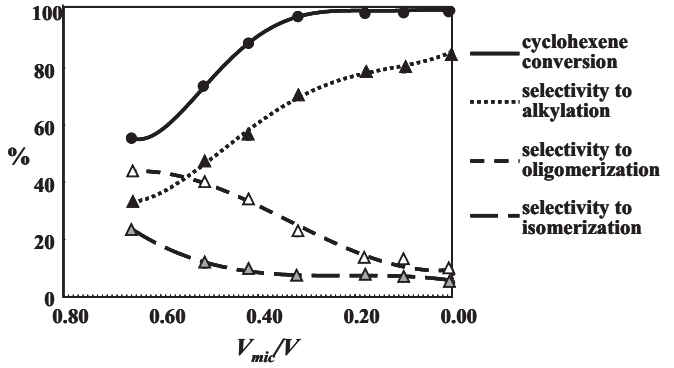

Fig. 11. Catalytic activity of parent and recrystallized mordenites in naphthalene cyclohexylation as a function of V_{mic}/V ratio. Reaction conditions: $T = 160\,^{\circ}C$, $P = 10$ atm, $WHSV_N = 0.5\ h^{-1}$, molar ration of CH:N:N_2 = 1:1:10, TOS = 3 h.

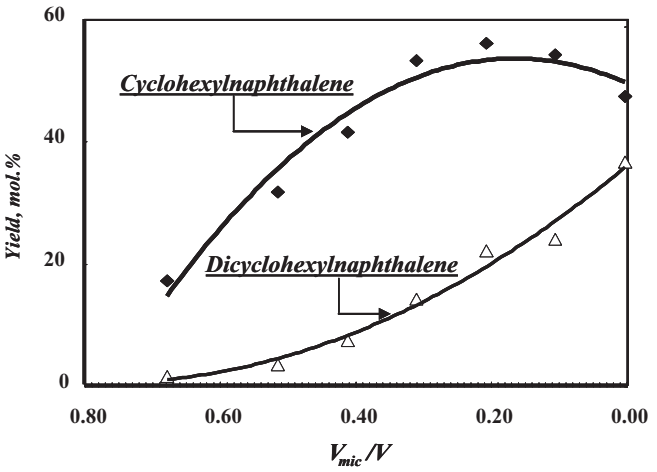

Fig. 12. The yields of mono- and disubstituted naphthalenes obtained during naphthalene cyclohexylation over parent and recrystallized mordenites as a function of V_{mic}/V ratio. Reaction conditions: $T = 160\,^{\circ}C$, $P = 10$ atm, $WHSV_N = 0.5\ h^{-1}$, molar ration of CH:N:N_2 = 1:1:10, TOS = 3 h.

The parent mordenite shows the lowest conversions of naphthalene and cyclohexene, which are noticeably different and reach 10% and 55%, respectively (Table 2). The main products over this catalyst are C_{12} oligomers (Fig. 11). The alkylation selectivity reaches only 33%, monoalkylation being predominant. The low alkylation selectivity and high CHN/DCHN ratio points to a strong steric hindrance for the formation of bulky alkylnaphthalenes inside the mordenite micropores. Thus, naphthalene alkylation takes place mostly on the external surface and at the pore mouths of the mordenite crystals, whereas oligomerization takes place on both the internal and external surfaces. A significant difference of acid sites concentration on the external and internal surfaces could explain the sharp difference in conversions of the two reactants and the higher oligomerization selectivity.

After the recrystallization in mild conditions (sample ReMOR-0.5 Table 2, Fig. 11), the naphthalene conversion increases by a factor of two, leading to higher alkylate yield. The sharp increase of alkylation selectivity is accompanied by a decrease of the methylcyclopentenes selectivity, whereas the oligomerization selectivity does not change significantly. Thus, the selectivity increase over ReMOR-0.5 is most probably due to an increase of naphthalene alkylation with methylcyclopentenes, but not to the suppression of oligomerization.

Further recrystallization (samples ReMOR-0.4 and ReMOR-0.3) resulting in higher mesoporosity, leads to a further increase of naphthalene and cyclohexene conversions (Fig. 11). At $V_{micro}/V = 0.3$, the cyclohexene conversion reaches 100%, whereas naphthalene conversion increases almost linearly with the ACI index. Starting from H/ReMOR-0.4, the increase in alkylation selectivity can be attributed to the suppression of oligomerization. Thus, selectivity to oligomers starts to decrease, whereas selectivity to isomerization products remains constant at V_{mic}/V higher than 0.4 (Fig. 11). The increase of alkylation at the expense of oligomerization can be accounted for by the easier transport of bulky naphthalene molecules provided by the mesopores.

Over the samples with high recrystallization degree, alkylnaphthalenes selectivity reaches 80–85%, while oligomers selectivity does not exceed 10–15% (Table 2). The alkylnaphthalenes production levels off for samples ReMOR-0.2 to ReMOR-0. On the contrary, selectivity to mono- and disubstituted alkylation products varies considerably (Table 2): while the amount of monosubstituted products starts to decrease on the catalysts with high recrystallization degrees, the contribution of dialkylnaphthalenes increases continually.

The monoalkylnaphthalenes and dialkylnaphthalenes yields over recrystallized mordenites are compared in Fig. 12. The highest monoalkylnaphthalenes yield is reached over composite micro–mesoporous material ReMOR-0.2. Increasing the recrystallization degree results in higher contribution of disubstituted products at the expense of monoalkylnaphthalenes.

In summary, the catalytic data highlight that micro/mesoporous materials prepared by mordenite recrystallization exhibit improved catalytic performances with respect to the parent mordenite. The best catalytic performance is achieved over composite micro–mesoporous materials with intermediate degree of recrystallization. The alkylnaphthalenes and monoalkylnaphthalenes yields over these catalysts reach 80% and 58%, respectively.

4. Conclusions

(1) Micro/mesoporous composite materials with different levels of micro- and mesoporosity were prepared by recrystallization of mordenite using a two-step procedure including (i) its partial destruction in a NaOH aqueous solution and (ii) its hydrothermal treatment in the presence of cethyltrimethylammonium bromide. It is demonstrated that the relative levels of micro- and mesoporosity can be tuned easily by adjusting the NaOH concentration in the first step.

(2) The investigation of the structural, textural and acidic properties of the materials obtained points to the following changes occurring during recrystallization:
   - recrystallization in mild conditions results in the creation of mesopores in zeolitic crystals but does not affect significantly the amount and strength of the acid sites;
   - the increase of the degree of recrystallization leads first to partial, and then to complete transformation of mordenite into MCM-41 accompanied by a gradual decrease of the amount and strength of the acid sites, while their accessibility increases drastically.

(3) Micro/mesoporous materials obtained by recrystallization of mordenite show superior catalytic performances (activity, stability and selectivity) in the alkylation of naphthalene with cyclohexene due to an improved accessibility of their active sites and an easier transport of bulky molecules provided by mesopores. The best catalytic performance is achieved with composite micro–mesoporous materials possessing an intermediate degree of recrystallization. The yield of alkylnaphthalenes over these materials reaches 80%, while the yield of monoalkylnaphthalenes is up to 58%.

Acknowledgement

Financial support by Total S.A. is gratefully acknowledged.

References

[1] S. van Donk, A.H. Janssen, J.H. Bitter, K.P. de Jong, Catal. Rev. 45 (2003) 297.
[2] Y. Tao, H. Kanoh, L. Abrams, K. Kaneko, Chem. Rev. 106 (2006) 896.
[3] J. Pérez-Pariente, I. Diaz, J. Agúndez, C. R. Chim. 8 (2005) 569.
[4] J. Čejka, S. Mintova, Catal. Rev. Sci. Eng. 49 (2007) 457.
[5] K. Egeblad, Cr.H. Christensen, M. Kustova, Cl.H. Christensen, Chem. Mater. 20 (3) (2008) 946.
[6] M. Ogura, Catal. Surv. Asia 12 (2008) 16.
[7] R. Dutartre, L.C. Menorval, F. Di Renzo, D. McQueen, F. Fajula, P. Schulz, Micropor. Mater. 5/6 (1996) 311.
[8] H. Ajot, J.F.J. Lynch, F. Raatz, P. Caullet, Stud. Surf. Sci. Catal. 62 (1991) 583.
[9] D. McQueen, B.H. Chiche, et al., J. Catal. 161 (2) (1996) 587.
[10] J.C. Groen, J.A. Moulijn, J. Pérez-Ramírez, J. Mater. Chem. 16 (2006) 2121.
[11] J.C. Groen, L.A.A. Peffer, J.A. Moulijn, J. Pérez-Ramírez, Chem. Eur. J. 11 (2005) 4983.
[12] C.H. Jacobsen, C. Madsen, J. Houzvicka, I. Schmidt, A. Carlssson, J. Am. Chem. Soc. 122 (2000) 7116.
[13] Y. Liu, W. Zhang, T.J. Pinnavaia, J. Am. Chem. Soc. 122 (2000) 8791.
[14] L. Huang, W. Guo, P. Deng, Z. Xue, Q. Li, J. Phys. Chem. 104 (2000) 2817.
[15] K.R. Kloestra, H. van Bekkum, J.C. Jansen, Chem. Commun. 2281 (1997).
[16] D.T. On, S. Kaliagine, Angew. Chem. Int. Ed. 40 (2001) 3248.
[17] D.T. On, D. Lutic, S. Kaliagine, Micropor. Mesopor. Mater. 44 (2001) 435.
[18] D.T. On, S. Kaliagine, Angew. Chem. Int. Ed. 41 (2002) 1036.
[19] I.I. Ivanova, A.S. Kuznetsov, V.V. Yuschenko, E.E. Knyazeva, Pure Appl. Chem. 76 (2004) 1647.
[20] S. Inagaki, M. Ogura, T. Inami, Y. Sasaki, E. Kikuchi, M. Matsukata, Micropor. Mesopor. Mater. 74 (2004) 163.
[21] I.I. Ivanova, A.S. Kuznetsov, O.A. Ponomareva, V.V. Yuschenko, E.E. Knyazeva, Stud. Surf. Sci. Catal. 158 (2005) 121.
[22] I.I. Ivanova, E.E. Knyazeva, Patent RF. No. 2282587 (2006).
[23] I.I. Ivanova, O.A. Ponomareva, E.E. Knyazeva, V.V. Yuschenko, E.S. Timoshin, E.V.Asachenko, Patent RF. No. 2288034 (2006).
[24] V.V. Ordomsky, V.Y. Murzin, Yu.V. Monakhova, Y.V. Zubavichus, E.E. Knyazeva, N.S. Nesterenko, I.I. Ivanova, Micropor. Mesopor. Mater. 105 (2007) 101.
[25] G.K. Williamson, W.H. Hall, Acta Metall. 1 (1953) 22.
[26] F. Thibault-Starzyk, I. Stan, S. Abelló, A. Bonilla, K. Thomas, C. Fernandez, J.P. Gilson, J. Perez-Ramirez, J. Catal. 264 (2009) 11–14.
[27] A. Vimont, F. Thibault-Starzyk, M. Daturi, Chem. Soc. Rev. 39 (2010) 4928.
[28] I.I. Ivanova, A.S. Kuznetsov, E.E. Knyazeva, F. Fajula, J.P. Gilson, to be published.
[29] B. Gil, S.I. Zones, S-J. Hwang, M. Bejblova, J. Cejka, J. Phys. Chem. C 112 (2008) 2997.
[30] C. Fernandez, I. Stan, J.P. Gilson, K. Thomas, A. Vicente, A. Bonilla, J. Pérez-Ramírez, Chem. Eur. J. 16 (2010) 6224.